International Journal of Thermal Sciences 49 (2010) 1197–1208

Contents lists available at ScienceDirect

International Journal of Thermal Sciences

journal homepage: www.elsevier.com/locate/ijts

Optimal parameters for pulsed gas tungsten arc welding in partially and fully penetrated weld pools

A. Traidia [a,b], F. Roger [a,*], E. Guyot [b]

[a] Unite de Mécanique, Ecole Nationale Superieure des Techniques Avancées, Chemin de la Hunière, 91761 Palaiseau cedex, France
[b] AREVA NP, Centre Technique Soudage, BP 4001 Saint Marcel, 71320 Chalon sur saône cedex, France

ARTICLE INFO

Article history:
Received 28 July 2009
Received in revised form
18 January 2010
Accepted 18 January 2010
Available online 23 February 2010

Keywords:
Arc welding
Pulsed current
Weld pool
Heat transfer
Fluid flow

ABSTRACT

In the present paper, a numerical model of spot pulsed current GTA welding for partially and fully penetrated weld pools is presented. Heat transfer and fluid flow in the weld pool driven by the combination of electromagnetic force, buoyancy force, surface tension gradient and latent heat are included in our model. A new formulation of the electromagnetic problem is introduced to take into account eddy current in the weld pool. The shape of the free deformable surface under the action of pulsed arc force is also handled after the magneto-hydrodynamic calculation.

The numerical model was applied to 304 stainless steel welding. We compare the influence of various pulsed welding parameters such as pulse frequency and current ratio on the weld quality. Experimental study is conducted to compare our numerical prediction with welding macrographies. It shows a good agreement of the model.

1. Introduction

Currently, the application of arc welding takes a leading position among other methods of welding. However arc welding introduces stress concentration, residual stresses and distortion. To get a good prediction of weld quality after welding many numerical models were developed [1–4] with the aim to predict thermal field which is strongly coupled with the fluid flow in the weld pool, and then the resulting thermo-metallurgical and mechanical behaviour of the structure. It is well known that the fluid flow coupled to the heat transfer in the weld pool strongly affect the final weld characteristics such as weld dimensions, temperature gradients and then microstructure.

Pulsed current GTA welding is widely used in welding with semi-automatic and automatic welding equipment. This process has been reported to have great advantages such as improving arc stability, avoiding weld cracks and reducing thermal distortion and residual stresses by the reduction of the total heat input [5]. Some experimental studies were conducted to determine the influence of pulsed current parameters on the welded joint [6,8]. An analytical model of the heat flow during pulsed welding is also available [7]. However, up to the present, far less work have been conducted on the numerical simulation of heat transfer and fluid flow in pulsed current GTA welding. Kim and Na [9] used the finite difference method with curvilinear coordinate system to calculate the heat transfer and the fluid flow in the weld pool of an axisymmetric disk. Wu and Zheng [10], on the other hand used also finite difference method to deal with the problem of moving torch, but in both cases, only partially penetrated weld pools are considered, due to the complexity of the coupling between the top and bottom free surfaces, and the electromagnetic field was computed as a stationary field by computing the electric potential. However under time pulsed conditions, the electromagnetic forces could be different from that of a constant current, since the variation of current induces a variation of the magnetic field, which creates itself an “eddy current”. The electromagnetic problem becomes a time-dependent problem depending on the frequency of the current.

An axisymmetric finite element model is proposed in this study to simulate the behaviour of fluid flow and heat transfer in the weld pool under pulsed current conditions. Comsol Multiphysics software is used to compute all the governing equations. Full penetrated weld pools are also considered. A new formulation of the electromagnetic field is introduced using the time-dependent magnetic field. The shape of the deformable free surface is also taken into account in a one way with the magneto-hydrodynamic

* Correspondence to: F. Roger, Ecole Nationale Superieure des Techniques Avancées, Mechanical department, Chemin de la Huniere, 91120 Palaiseau, France. Tel.: +33 169 319 815; fax: +33 169 319 906.
E-mail address: frederic.roger@ensta.fr (F. Roger).

1290-0729/$ – see front matter © 2010 Elsevier Masson SAS. All rights reserved.
doi:10.1016/j.ijthermalsci.2010.01.021

coupling. In industry the impact of the pulse parameters on the final weld quality is still empirical. Here a great effort has been made to study the influence of the main parameters of the pulse on the weld dimensions, thermal cycles and temperature gradients.

2. Mathematical formulation and governing equations

Fig. 1 shows a representation of the weld pool under the action of the arc plasma. Fluid flow in the pool is driven by a combination of buoyancy, electromagnetic, surface tension and arc pressure. Our transient model is based on the finite element method to compute the final weld shape, the fluid flow and the thermal field in the weld pool. In order to simplify the problem, the following assumptions are considered:

- The study is restricted to GTA spot welding, then we use an axisymmetric coordinate system.
- The flow is laminar and incompressible due to the small size of the weld pool, however gravity force is taken into account using the boussinesq approximation.
- The thermal gradient of surface tension is temperature dependent, and the latent heat of fusion is taken into account.
- The magnetic field is time dependent and not a superposition of the top and bottom stationary solutions.
- The coupling between the MHD calculus and the free surface is in one way, that is to say the free surface doesn't affect the calculated thermal field.

2.1. The hydrodynamics problem

Based on the above assumptions, the classical Navier–Stokes equations which governs the fluid flow in the weld pool can be expressed as follows:

(1) Conservation of mass

$$\nabla\cdot\vec{v} = 0 \tag{1}$$

(2) Conservation of momentum

$$\rho\left(\frac{\partial\vec{v}}{\partial t} + \vec{v}\cdot\nabla\vec{v}\right) = -\nabla p + 2\mu\nabla\cdot D(\vec{v}) + \vec{F}_v$$

$$D(\vec{v}) = \frac{1}{2}(\nabla\vec{v} + {}^t\nabla\vec{v}) \tag{2}$$

$\vec{F}_v$ represents body forces in the weld pool, it is the sum of Lorentz force and buoyancy force (Boussinesq approximation) and could be expressed as:

$$\vec{F}_v = \rho_0(1-\beta(T-T_{\text{ref}}))\vec{g} + \vec{j}\wedge\vec{B} \tag{3}$$

Where $\vec{v}$ is the velocity vector field in the weld pool, t is time, ρ is density, μ is viscosity, p is pressure field, g is gravity, T_{ref} is a reference temperature taken as the solidus temperature of the alloy, $\vec{j}$ is the current density vector and $\vec{B}$ is the magnetic field vector.

(3) Energy conservation

$$\rho C_p\frac{\partial T}{\partial t} + \rho C_p\vec{v}\cdot\nabla(T) = \nabla\cdot(\lambda\nabla T) + Q + \rho L_f\frac{df_L}{dt} \tag{4}$$

f_L is the liquid fraction, assumed to vary linearly with temperature in the mushy zone:

$$f_L = 1; \quad \text{if } T > T_L$$

$$f_L = \frac{T-T_s}{T_L-T_s}; \quad \text{if } T_s \le T \le T_L \tag{5}$$

$$f_L = 0; \quad \text{if } T < T_L$$

The equation of energy conservation could also be written as:

$$\rho C_p^{eq}\left(\frac{\partial T}{\partial t} + \vec{v}\cdot\nabla T\right) = \nabla\cdot(\lambda\nabla T) + Q \tag{6}$$

Where T is temperature, C_p is specific heat and $C_p^{eq} = C_p + L_f(\partial f_L/\partial t)$ is an equivalent specific heat which takes into account the latent heat of fusion L_f.

Formulating the thermal problem using C_p^{eq} is very interesting because the energy equation takes a classical form. The energy conservation is computed using the last formulation.

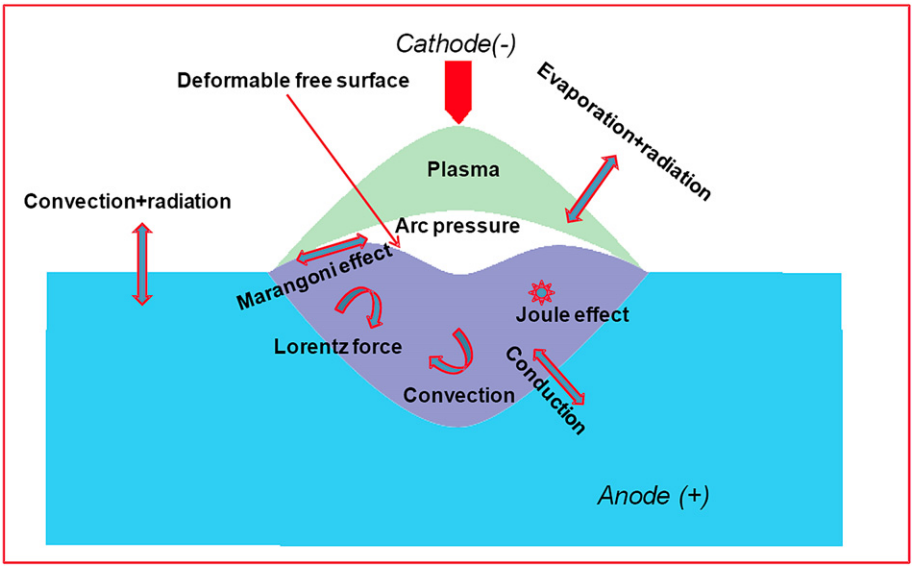

Fig. 1. Multiphysics coupling on a pulsed GTA welding.

In order to avoid round-off due to manipulations with large/small numbers and to assess the relative importance of terms in the model equations it is useful to rewrite the whole equations in dimensionless form. One must define reference quantities and related scales for time, pressure, length, temperature and velocity. Then we can introduce new dimensionless variables for the problem as following:

$$\begin{aligned} R &= \frac{r}{L_{\text{ref}}}; \quad Z = \frac{z}{L_{\text{ref}}} \\ \mathbf{V} &= \frac{\vec{v}}{V_{\text{ref}}}; \quad \tau = \frac{tV_{\text{ref}}}{L_{\text{ref}}} \\ P &= \frac{p}{L_{\text{ref}}V_{\text{ref}}^2}; \quad \Theta = \frac{T-T_0}{T_L-T_s} \end{aligned} \tag{7}$$

In our model we use $L_{\text{ref}} = 1$ mm and $V_{\text{ref}} = 1$ m/s Thus the momentum, mass and energy conservation equations could be rewritten as:

$$\begin{aligned} &-\nabla P + \frac{2}{R_e}D(\mathbf{v}) + \frac{F_v L_{\text{ref}}}{\rho V_{\text{ref}}^2} = \left(\frac{\partial \mathbf{V}}{\partial \tau} + \mathbf{V}\cdot\nabla\mathbf{V}\right) \\ &\nabla\cdot\mathbf{V} = 0 \\ &\rho C_p L_{\text{ref}} V_{\text{ref}}\left(\frac{\partial \Theta}{\partial \tau} + \mathbf{V}\nabla\Theta\right) = \nabla\cdot(\lambda\nabla\Theta) \end{aligned} \tag{8}$$

2.2. The electromagnetic problem

Under time pulsed conditions, the electromagnetic forces could be different from that of a constant current, since the variation of current during welding induces a variation of the magnetic field which creates eddy current in the weld pool. The electromagnetic field in the weld pool cannot be approximated by cyclic evolution of the two stationary solutions at the top and bottom currents. To get a good formulation of the problem, it is important to remind the fundamental laws of electromagnetism that could be written as follows:

$$\begin{aligned} &\nabla\cdot\vec{B} = 0; \quad \vec{B} = \nabla\times\vec{A} \\ &\vec{J}_e = \sigma\vec{E}; \quad \vec{E} = -\nabla V - \frac{\partial\vec{A}}{\partial t} \\ &\nabla\times\vec{E} = -\frac{\partial\vec{B}}{\partial t}; \quad \nabla\times\vec{B} = \mu_0\vec{J}_e + \mu_0\epsilon_0\frac{\partial\vec{E}}{\partial t} \end{aligned} \tag{9}$$

Where $\vec{B}$ is the magnetic field, $\vec{E}$ is the electric field, $\vec{J}$ is the current density, σ electrical conductivity, μ_0 and ϵ_0 are respectively vacuum permeability and vacuum permittivity. Considering the above equations the electromagnetic problem could be written as a function of the magnetic field $\vec{B}$ as follows:

$$\frac{\partial^2\vec{B}}{\partial t^2} + \frac{\sigma}{\epsilon_0}\frac{\partial\vec{B}}{\partial t} - \frac{1}{\mu_0\epsilon_0}\Delta\vec{B} = \vec{0} \tag{10}$$

Since the problem is axisymmetrical, only the θ-component of the magnetic field $\vec{B}$, and the r and z components of the current density $\vec{J}$ are considered. Thus the equation becomes:

$$\frac{\partial^2 B_\theta}{\partial t^2} + \frac{\sigma}{\epsilon_0}\frac{\partial B_\theta}{\partial t} + \frac{1}{\mu_0\epsilon_0 r^2}B_\theta - \frac{1}{\mu_0\epsilon_0}\Delta B_\theta = 0 \tag{11}$$

After solving the above equation the current density vector is obtained from the Ampere's law as follows:

$$J_r = \frac{-1}{\mu_0}\frac{\partial B_\theta}{\partial z}; \quad J_z = \frac{1}{\mu_0 r}\frac{\partial(rB_\theta)}{\partial r} \tag{12}$$

2.3. The free surface problem

Under the actions of gravitational force, arc pressure and surface tension acting on the weld pool, the free surface will form a shape that minimizes the total energy of surface. The well known stationary equation governing the free surface of the weld pool takes the following form:

$$P_a + \lambda - \rho g\phi = -\gamma\frac{r\phi_{rr} + \phi_r\left(1+\phi_r^2\right)}{\left(1+\phi_r^2\right)^{\frac{3}{2}}} \tag{13}$$

Where ϕ is the vertical displacement of the top surface of the weld pool, ϕ_r represents $\partial\phi/\partial r$, and P_a the arc pressure with its distribution given in Fig. 3(c). λ is a Lagrangian multiplier introduced to take into account the volume constraint under the free surface $\int_S 2\pi\phi(r)rdr = 0$. The above stationary equation is often used to determine the free surface shape under constant current welding [4]. In our study, in order to simplify the problem we only consider the free surface shape at the top and bottom times of the pulse.

2.4. Boundary conditions

Fig. 2 shows the two different geometric configurations used in this study for respectively partially and fully penetrated weld pools. In order to reduce time computing, each geometry is made of two subdomains with different mesh densities in each subdomain. For example, in the case of a partially penetrated weld pool, the electromagnetic and energy conservation equations are solved in the whole domain, i.e AEFG with a coarse mesh, however the momentum and mass conservation equations are solved only in the subdomain ABCD with a finer mesh size in the subdomain and in particular at the top surface where occurs high gradients.

For a partially penetrated weld pool (Fig. 2 left) the boundary conditions of the problem are listed as following:

(1) At the top surface of the workpiece (AB + BE)

$$J_r = \frac{-1}{\mu_0}\frac{\partial B_\theta}{\partial z} = J_0(r) \Leftrightarrow \frac{\partial B_\theta}{\partial z} = -\mu_0 J_0(r) \tag{14}$$

$$-k\frac{\partial T}{\partial z} = q_0(r) \tag{15}$$

Where $J_0(r)$ and $q_0(r)$ are respectively the current density and the heat flux which distributions are given in Fig. 3(a) and (b).

In addition, at the free surface (region AB) the surface tension or Marangoni-driven flow is described by adding the condition:

$$\mu\frac{\partial u}{\partial z} = f_L\frac{\partial\gamma}{\partial T}\frac{\partial T}{\partial r}; \quad v = 0 \tag{16}$$

With u radial velocity of the fluid flow.

The temperature coefficient of surface tension $\partial\gamma/\partial T$ for pure metals is negative, however the presence of sulfur in the weld pool can make the value of $\partial\gamma/\partial T$ positive. For liquid metals with $\partial\gamma/\partial T$ positive, the direction of the Marangoni stress on the surface of the weld pool is changed resulting in an inward fluid flow which affects the weld pool geometry. In the present study, the surface tension γ as a function of both temperature and sulfur activity is obtained from the developed formalism [11]:

$$\gamma = \gamma_m - A_\gamma(T-T_L) - R_g T\Gamma_s\ln(1+K(T)a_s) \tag{17}$$

$$K(T) = k_1\exp\left(-\frac{\Delta H_0}{R_g T}\right) \tag{18}$$

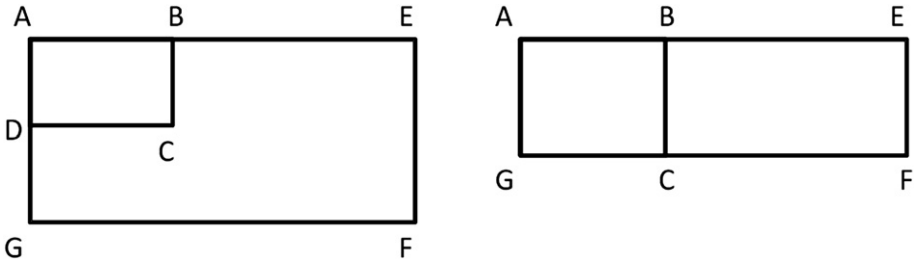

Fig. 2. Computational domains for partially (left) and fully (right) penetrated weld pools.

Where γ_m is the surface tension of the pure metal at the melting temperature, a_s is the activity of sulfur and T_L is the liquidus temperature. The other variables are classical physical quantities, the values are given in Table 1. The validity of the above equation for application in Stainless Steel has been demonstrated in [12,13].

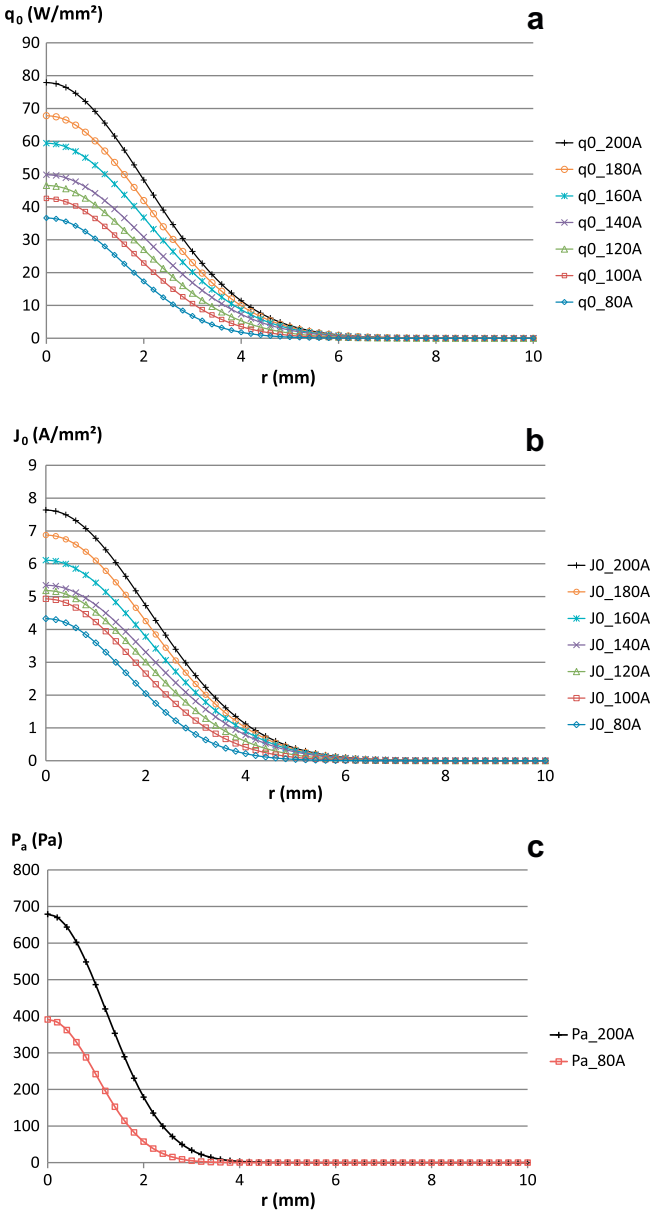

Fig. 3. (a): Heat flux at the top surface of the weld pool. (b): Current density at the top surface of the weld pool. (c): Arc pressure at the top surface of the weld pool.

By differentiating Eq. (17) with respect to temperature, the expression of $\partial\gamma/\partial T$ as a function of both temperature and sulfur activity can be obtained as:

$$\frac{\partial\gamma}{\partial T} = -A_\gamma - R_g\Gamma_s\ln(1+Ka_s) - \frac{Ka_s}{1+Ka_s}\frac{\Gamma_s\Delta H_0}{T} \tag{19}$$

(2) At the outer surface (EF). A convective boundary condition is applied;

$$-k\frac{\partial T}{\partial r} = h_0(T - T_0) \tag{20}$$

Where h_0 is the convective coefficient of heat transfer.

$$J_z = \frac{1}{\mu_0 r}\frac{\partial(rB_\theta)}{\partial r} = 0 \Leftrightarrow \frac{\partial(rB_\theta)}{\partial r} = 0 \tag{21}$$

(3) At the bottom surface (FG)

$$-k\frac{\partial T}{\partial z} = h_0(T - T_0) \tag{22}$$

$$J_z = 0 \Leftrightarrow \frac{\partial(rB_\theta)}{\partial r} = 0 \tag{23}$$

(4) Along the axisymmetrical axis (AD + DG)

$$-k\frac{\partial T}{\partial r} = 0 \tag{24}$$

$$B_\theta = 0 \tag{25}$$

$$u = 0 \tag{26}$$

Table 1
Material properties of AISI 304 stainless steel taken from [9].

Nomenclature	Symbol	Value
a_s	Activity of sulfur	0.0072 wt%
A_γ	Constant in surface tension gradient	3×10^{-4} N m^{-1} K^1
ρ_l	Density of liquid phase	6350 kg m^{-3}
ρ_s	Density of solid phase	7500 kg m^{-3}
T_l	Liquidus temperature	1723 K
Ts	solidus temperature	1673 K
C_{pl}	Specific heat of liquid phase	720 J kg^{-1} K^{-1}
C_{ps}	Specific heat of solid phase	602 J kg^{-1} K^{-1}
k_l	Thermal conductivity of liquid phase	20 W m^{-1} K^{-1}
k_s	Thermal conductivity of solid phase	26 W m^{-1} K^{-1}
μ	Viscosity	0.05 kg m^{-1} s^{-1}
σ	Electrical conductivity	7.7×10^5 Ω^{-1} m^{-1}
R_g	Gas constant	8314.3 J kg^{-1} mol^{-1} K^{-1}
ΔH_0	standard heat of adsorption	-1.88×10^8 J kg^{-1} mol^{-1}
Γ_s	Surface excess at saturation	1.3×10^{-8} J kg^{-1} mol^{-1} m^{-2}
γ_m	Surface tension at pure metal	1.943 N m^{-1}

(5) Along the solid interfaces (BC + CD)

$$u = v = 0 \tag{27}$$

It is important to notice that formulating the electromagnetic problem as function of the magnetic field $\vec{B}$ is very interesting, because the current density $\vec{J}$ is immediately obtained by a spacial differentiation. In fact the classical formulation of the problem in term of the electric potential ϕ implies an integration step of the current density $\vec{J}$ to obtain the magnetic field.

In the case of a fully penetrated weld pool (Fig. 2 right) the boundary conditions remain the same except for the penetration boundary (GC) where it is necessary to take into account the Marangoni condition:

$$\mu\frac{\partial u}{\partial z} = f_L\frac{\partial \gamma}{\partial T}\frac{\partial T}{\partial r}; \quad v = 0 \tag{28}$$

This makes the problem more complex because the two Marangoni conditions on the top and bottom of the weld pool are coupled by the fluid flow.

3. Results and discussion

Our spot pulsed GTAW model permits to us to study the influence of welding parameters on the fluid flow in the weld pool and the final weld shape. Indeed, surface tension depending on temperature coupled to Marangoni effect produces complex fluid flow with vortices which produces quite different weld pool shapes according to welding parameters. In the following paragraph, we will first present the results of the developed model for partially and fully penetrated pulsed GTAW welding, in a second part we will compare welding under constant current with pulsed current, and finally the model will be used to understand the effect of pulse parameters such as current ratio (I_p/I_b) and pulse frequency on weld pool shape and thermal field.

The numerical model was applied to AISI 304 stainless steel welding containing 72 ppm sulfur. Table 1 lists the physical properties for AISI 304 ss taken from literature [9]. The temperature dependent surface tension and its thermal gradient obtained from equation are represented in Fig. 4(a) and (b).

3.1. Comparison between partially and fully penetrated weld pool

In this part, we present time evolution of the GTAW weld pool for 4 and 10 mm thickness plates. Operating parameters are the same for both cases, so the thin plate will have a fully penetrated weld pool. The pulsed GTAW spot parameters are listed in Table 2.

3.1.1. Results for partial penetration

It is well known that the fluid flow and heat transfer in the weld pool are dominated by Marangoni convection, which is due to the temperature gradient of surface tension $\partial\gamma/\partial T$. Fig. 4(b) shows that $\partial\gamma/\partial T$ is positive until temperature reaches approximately a critical temperature $T_c = 2300$ K with a maximum of $8.52\cdot10^{-4}$ N m^{-1} K^{-1}; it then becomes negative for higher temperatures and reaches a minimum of $-2.75\cdot10^{-4}$ N m^{-1} K^{-1}.

Fig. 5(a) and (b) show the time evolution of the calculated weld pool at the end of each background time and each peak time for the total heating duration. In each figure it is represented the velocity field and the streamlines inside the molten pool in order to identify vortices. First it is important to notice that in each figure it appears clearly two vertice; a clockwise vortex near the center of the weld pool resulting in an outward fluid flow at the surface, the other one is a counterclockwise vortex near the solidification point resulting in an inward fluid flow at the surface of the weld pool.

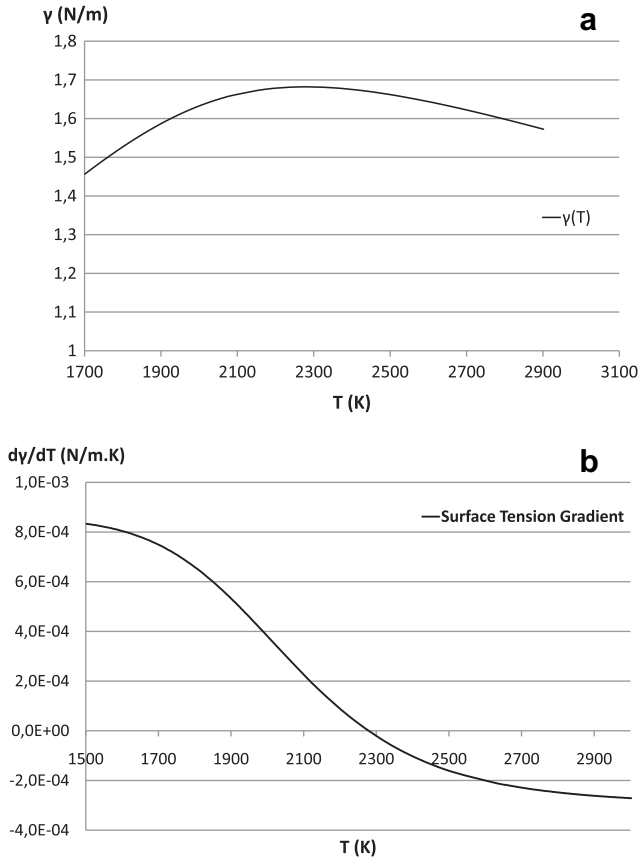

Fig. 4. (a): Surface tension as function of temperature for 72 ppm sulfur AISI 304. (b): Surface tension gradient for 72 ppm sulfur AISI 304.

It is also seen that at each background time the counterclockwise vortex is clearly dominant, which induces a deeper weld pool. Whereas, at each peak time the clockwise vortex is dominant which creates a wider weld pool.

This phenomenon is simply due to the $\partial\gamma/\partial T$ evolution. In fact as it is shown in Fig. 6 at background time the temperature varies from the liquidus temperature $T_L = 1723$ K to about $T_{max} = 2650$ K, which is above the critical temperature T_c shown previously in $\partial\gamma/\partial T$ evolution, this explains the existence of two vertice; a clockwise one corresponding to the region where $\partial\gamma/\partial T > 0$ and a counterclockwise vortex corresponding to the domain where $\partial\gamma/\partial T > 0$. Moreover, T_{max} is closer to T_c, then the region with $\partial\gamma/\partial T > 0$ is more important which explains the domination of the counterclockwise vortex. Whereas, at peak time, Fig. 6 shows that T_{max} is above 3000 K, then the region with $\partial\gamma/\partial T > 0$ becomes more important which causes the domination of the clockwise vortex.

The evolution of weld pool depth and half width a function of time is shown in Fig. 7. As seen in this figure the weld pool

Table 2
Pulsed welding parameters.

Nomenclature	Symbol	Value
I_p	Peak pulse current	200 A
I_b	Background current	80 A
t_p	Peak pulse duration	0.25 s
t_b	Background duration	0.25 s
f	Pulse frequency	2 Hz
t_t	Total heating duration	3.5 s
n_p	Number of periods	7

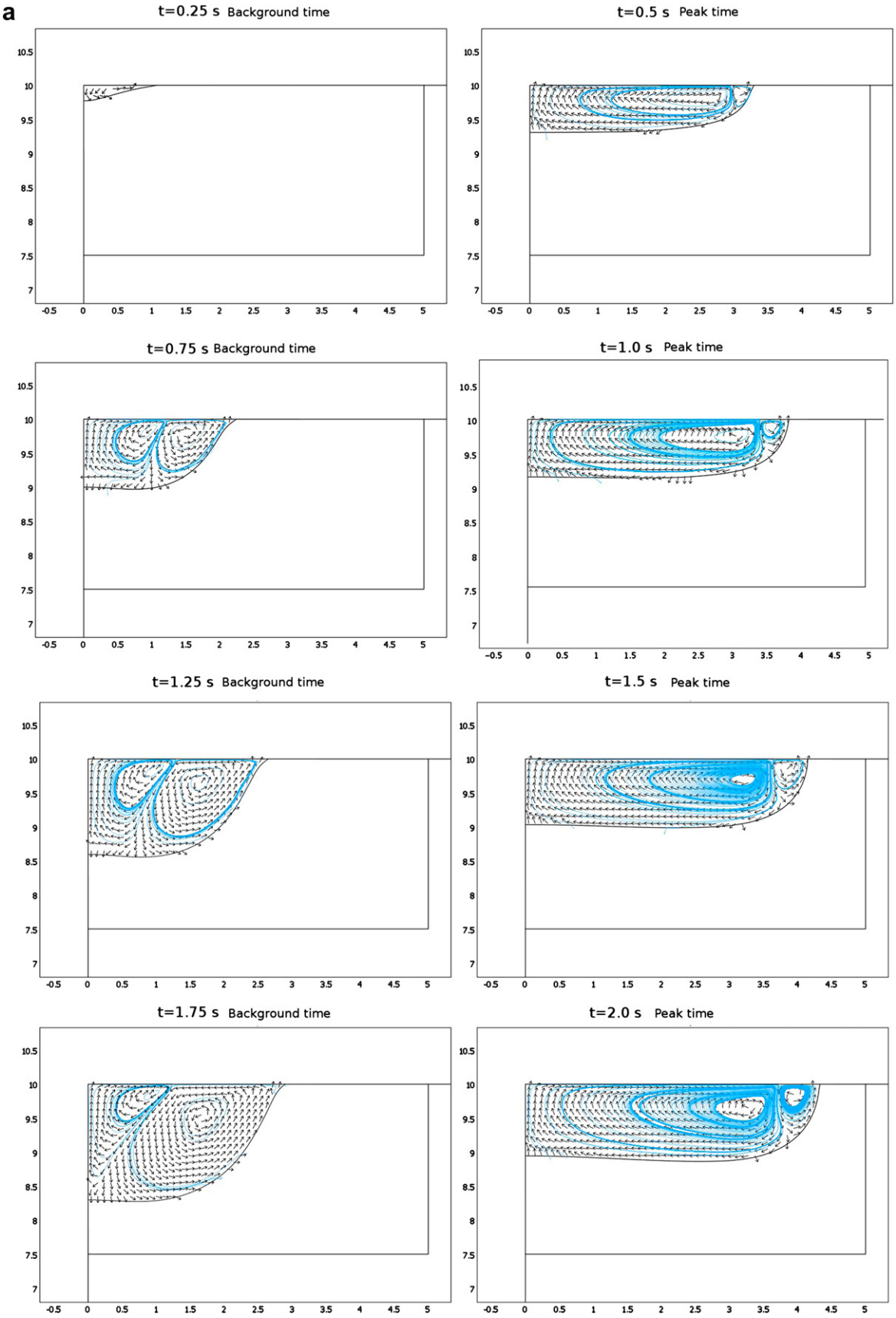

Fig. 5. (a): Time evolution of the weld pool and streamlines for a 80/200 A pulsed current during the four first periods. (b): Time evolution of the weld pool and streamlines for a 80/200 A pulsed current welding during the three last periods.

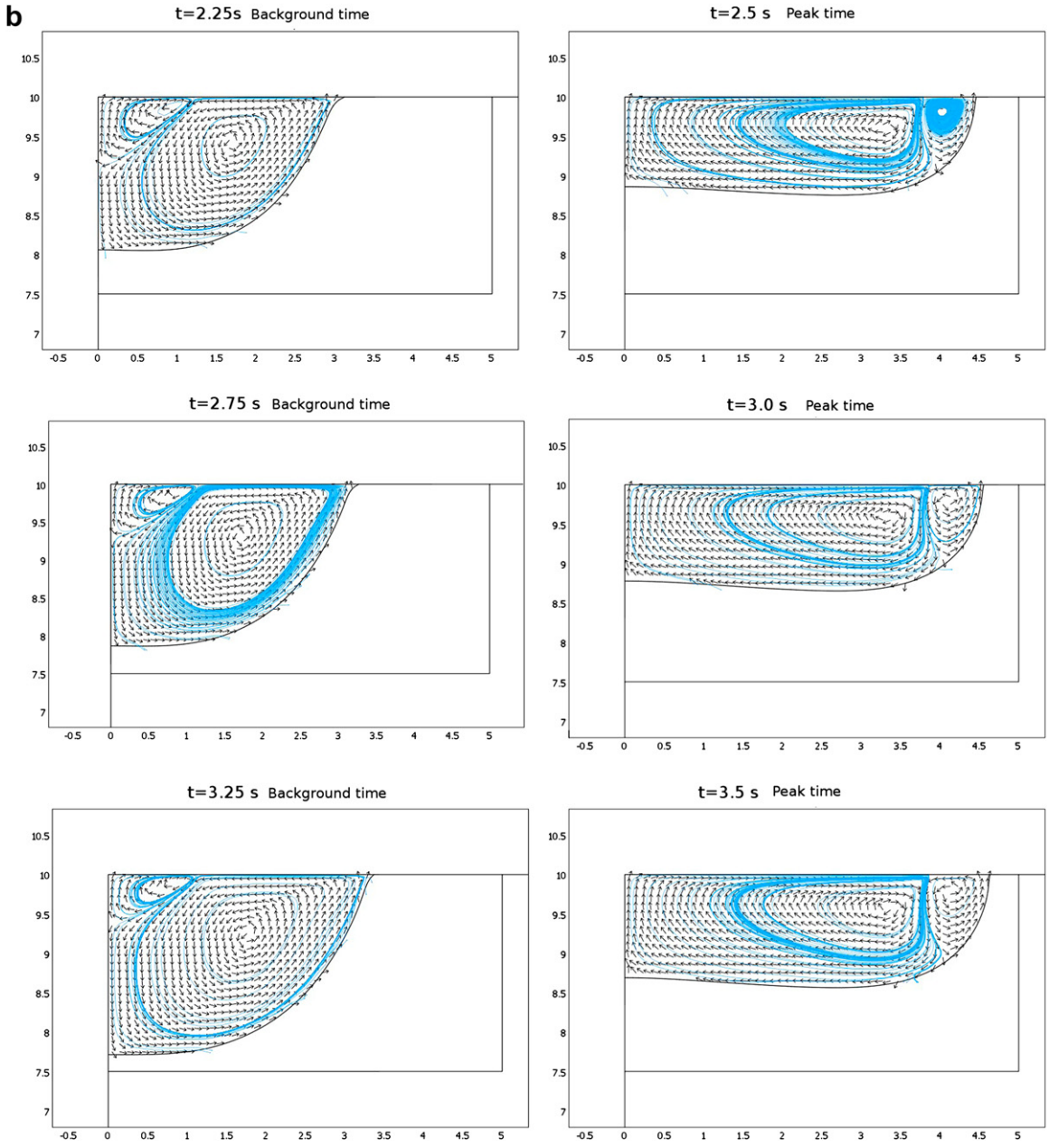

Fig. 5. *(Continued).*

dimensions represents a very clear change at each peak or background time, it illustrates perfectly the domination of each vortex discussed above. Since the clockwise vortex is dominant at peak time, the outward fluid flow at the top surface induces an increasing of the weld pool width, while its depth is decreasing, during the background time, conversely; the width is decreasing while the depth is increasing which illustrates the domination of the counterclockwise vortex.

The velocity field at the top surface of the weld pool plays an important role to what happens inside the molten pool. Fig. 8 shows the evolution of the radial velocity u as a function of the radius r at the top surface. The two curves are plotted at the end of the peak and background times for the last heating period. As it was predicted, in each curve there are two regions; one region in which the radial velocity is negative, the other one correspond to a positive velocity. During the background time the radial velocity is predominantly negative with a maximum of 35 cm s^{-1}, this velocity becomes predominantly positive during the peak time with a maximum of 40 cm s^{-1}. Globally, the two evolutions are similar but shift in time.

Fig. 9 shows the free surface shape under the action of the arc pressure for the peak current 200 A and background current 80 A. As seen the free surface is deformed under the action of arc pressure, gravity and surface tension. The maximum depression reached for the peak current is about 0.28 mm whereas it is about 0.09 mm for the background currents. These values are very small compared to the weld pool dimensions, for example the ratio (ϕ/width) for the peak current is about 0.06. This explains the one side coupling considered between the free surface deformation and the hydrodynamics computation.

To obtain a three-dimensional representation of the results, needed to compute the residual deformations where the clamping

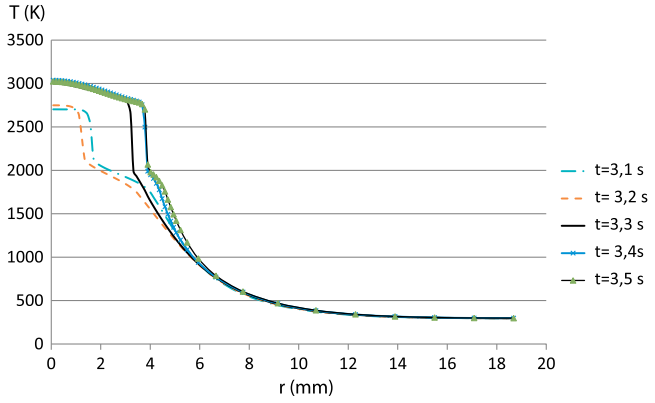

Fig. 6. Temperature at the top side of the plate for the last period; transition between the background and peak times.

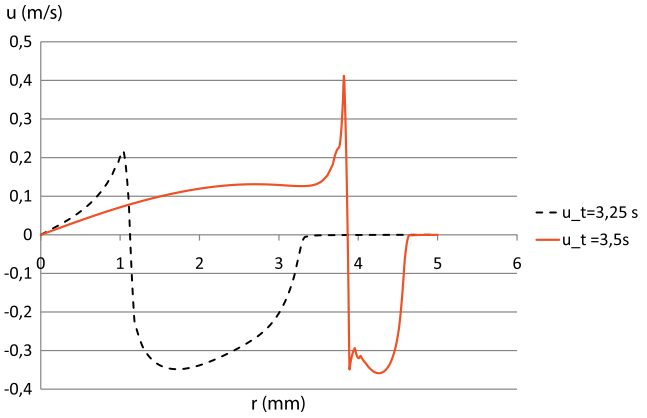

Fig. 8. Radial velocity at the top surface of the weld pool for the last peak and background times.

could make the problem non-axisymmetrical, we have used an algorithm that projects all the computed quantities into a three-dimensional disk. Fig. 10 represents the weld pool at the end of the heating duration and some isothermal lines. As the end of heating corresponds to a peak time, we could easily see the domination of the clockwise vortex.

3.1.2. Results for full penetration

In the case of a fully penetrated weld pool, the thickness of the plate was reduced from 10 mm to 4 mm to ensure the full penetration. We used the same process variables as the 10 mm thick plate welding.

Fig. 11 shows the time evolution of the weld pool depth, the top and bottom width. The evolutions seem to be similar to a partially penetrated weld pool except the fact that the bottom width remains at zero until the fully penetration occurs. A very remarkable point is that after the achieving of the full penetration the width on the top surface has an opposite evolution compared to the width on the bottom side. This is simply due to the sign of the surface tension gradient.

The weld pool shape at the end of heating is shown in Fig. 12. It is also represented the velocity field and the streamlines. We could easily identify three vertice inside the molten pool; the two vertice at the top correspond to the classical vertice discussed previously, the clockwise one is dominating since the end of heating corresponds to a peak time. The new vortex at the bottom is due to the Marangoni effect at the bottom side of the weld pool. The reason why there is only one vortex at the bottom is that the maximum of temperature at this side is about 2000 K which is under the critical temperature $T_c = 2300$ K. Thus the surface tension gradient $\partial\gamma/\partial T$ is positive everywhere, this results in a single counterclockwise vortex at the bottom.

3.2. Comparison between constant current and pulsed current

Pulsed welding is here compared to a constant welding current which produces approximately the same weld pool geometry (depth and width). This will demonstrate the ability of pulsed welding to produce the same penetration than a constant current welding which needs more welding energy. Then, we will expect to have less residual distortion with pulsed current welding.

Fig. 13 represents the time evolution of the weld pool width and depth for a 10 mm thick plate, under a 80/200 A pulsed current welding compared to a 170 A continuous current welding. As it is seen in this figure the 170 A continuous current produces almost the same weld pool dimensions as the 80/200 A pulsed current. However over 3.5 s the continuous current corresponds to a total heating energy of about 5867 J, while the pulsed current is equivalent to 4565 J, so the reduction of energy is significant.

In other words, for a given weld pool shape (width and depth) we reduce the welding energy by 22% when using pulsed current welding. Then the residual distortions and stresses are expected to be significantly reduced.

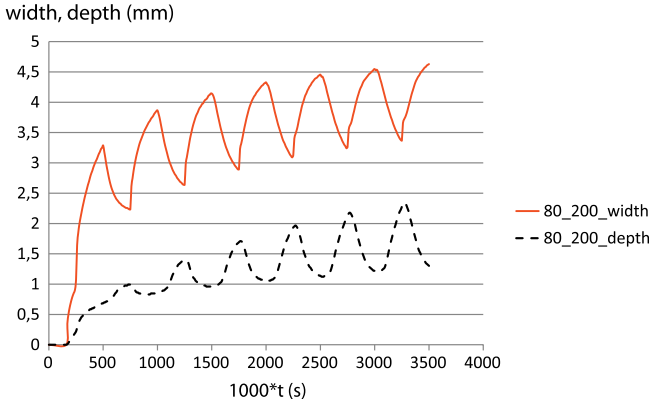

Fig. 7. Time evolution of width and depth of the weld pool for a 80/200 A pulsed current welding at 2 Hz.

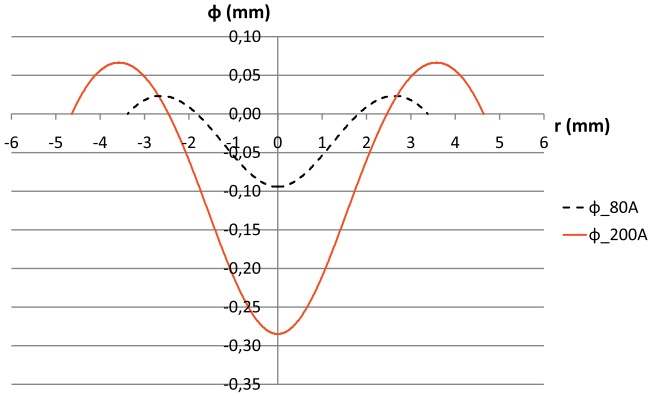

Fig. 9. Free surface shapes for the peak (red) and background (blue) currents. (For interpretation of the references to colour in this figure legend, the reader is referred to the web version of this article.)

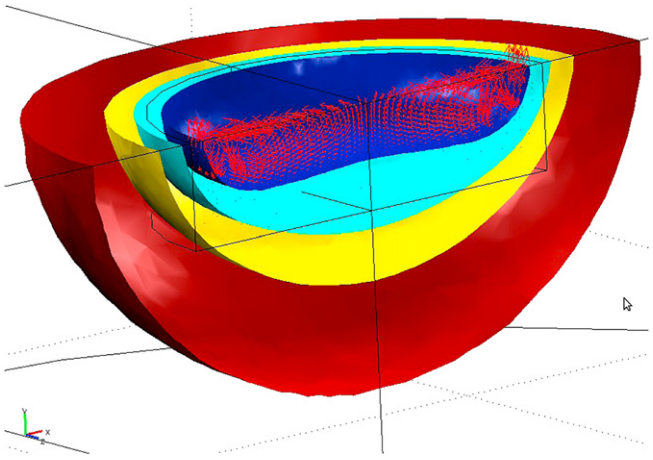

Fig. 10. Three-dimensional projection of the velocity field and isothermal lines (1723 K, 1300 K, 1000 K, 600 K) at the end of calculation.

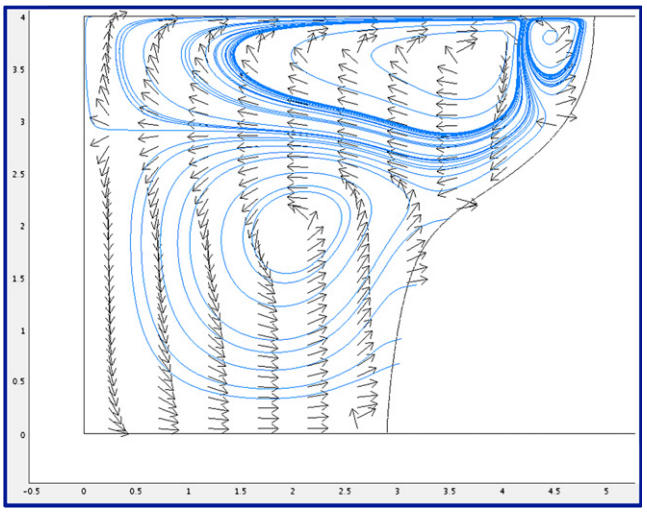

Fig. 12. Weld pool shape, normalized velocity field and streamlines for a fully penetrated weld pool at the end of calculation.

3.3. *Effect of pulse parameters on weld pool time evolution*

The aim of welder is to choose the best welding parameters to maximise welding penetration and to minimize thermal gradient to reduce the residual distortion and stresses. Pulsed current welding is then an optimal choice. However, the welding parameters are more complex to define and up to today the choice of parameters remains empirical. In this section, we will try to use our model in order to understand the influence of current ratio and pulse frequency on the shape of the weld pool and the thermal gradients.

3.3.1. *Influence of the current ratio at constant energy*

Using two levels of current during pulsed welding produces high thermal gradients because the heating by arc plasma evolved periodically with radius variation. Here, we study at constant total welding energy, with a 140 A mean current but with three different current variations (120/160 A; 100/180 A and 80/200 A) the induced weld pool shape and the corresponding thermal field history. Fig. 14(a) shows the time evolution of welding current, the corresponding measured voltage is given in Fig. 14(b), it is important to notice that the three cases have the same pulse frequency (2 Hz), moreover the peak pulse duration t_p is equal to the background duration t_b, this leads to understand only the effect of the current ratio I_p/I_b. Simulated weld shapes after solidification for the three cases are compared to macrographs and show a very good predictions by our model.

The time evolution of the weld pool width and depth for the three welding cases is given in Fig. 15 in which the case of the continuous mean current of 140 A is also represented for comparison. The first remarkable thing is that the three pulsed cases produce a deeper and wider weld pool than the mean current. This suggests saying that for a given level of welding energy, it is more interesting to use a pulsed current welding. On the other hand the depth difference between the three pulsed cases seems to be higher than the width difference. In fact it is clearly seen that the 80/200 A case produces a deeper weld pool than the others, this is caused by the fact that the background current is smaller, which leads to have a positive surface tension gradient resulting in an inward fluid flow near the center of the plate. This inward flow induces a deeper weld pool.

From the temperature field, the comparison between the three pulsed cases and the mean current is given in Fig. 16, showing the evolution of the top side temperature as a function of radius at the last time. As it was expected the pulsed cases induce a higher temperature at the center of the plate. The interesting point is that far from the molten pool, there is no difference between the whole cases. This may be due to the fact that all cases have the same welding energy.

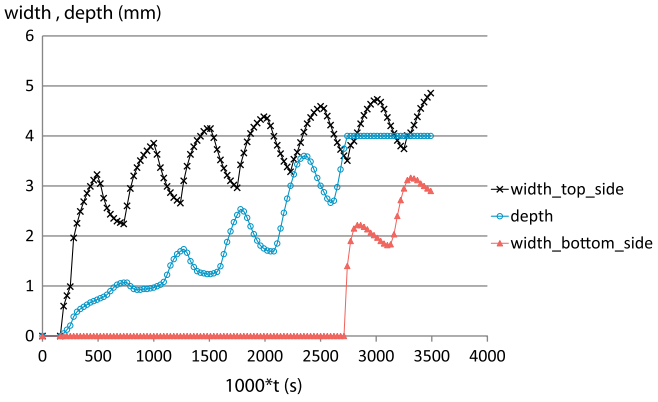

Fig. 11. Time evolution of the depth, width on the top and width on the bottom for a fully penetrated weld pool.

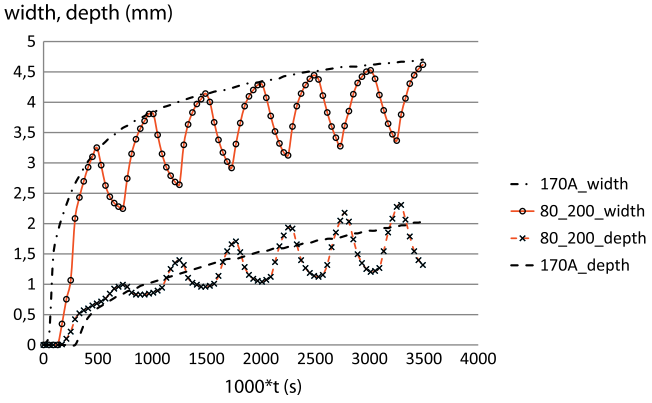

Fig. 13. Comparison of weld pool dimensions between pulsed and continuous current welding.

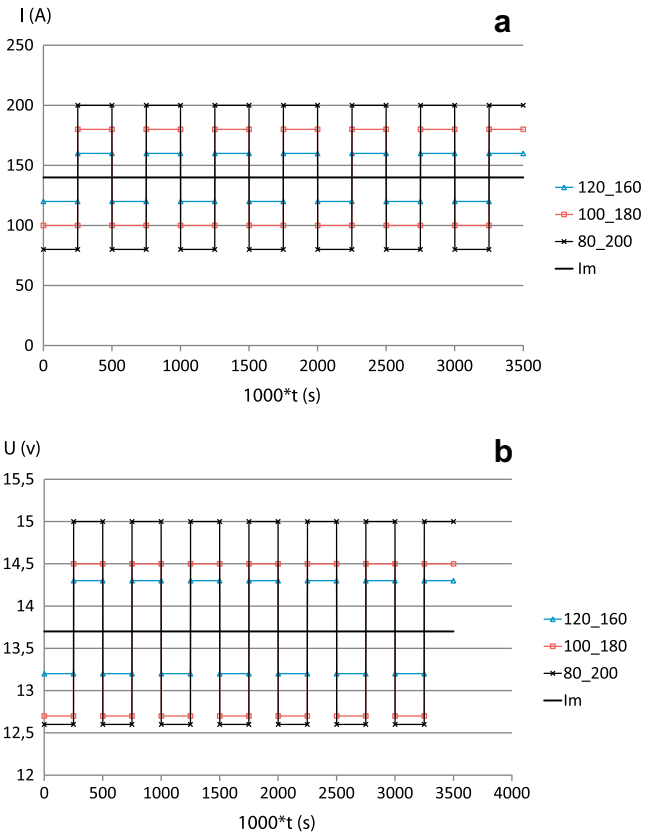

Fig. 14. (a): Three current evolutions at constant energy. (b): Corresponding measured voltage of each current.

As it was said previously the pulsed current cases produce a wider and deeper weld pool than the mean current, however they induce higher thermal gradients caused by the periodic transition between two levels of current. To emphasize this difference, the Fig. 17 shows the time evolution of the thermal gradients near the solidification point for the whole cases. This point is located in the Heat Affected Zone where the main residual strains are concentrated. As seen in this figure, until the time $t = 1$ s the mean current 140 A induces a higher thermal gradients than the pulsed cases.

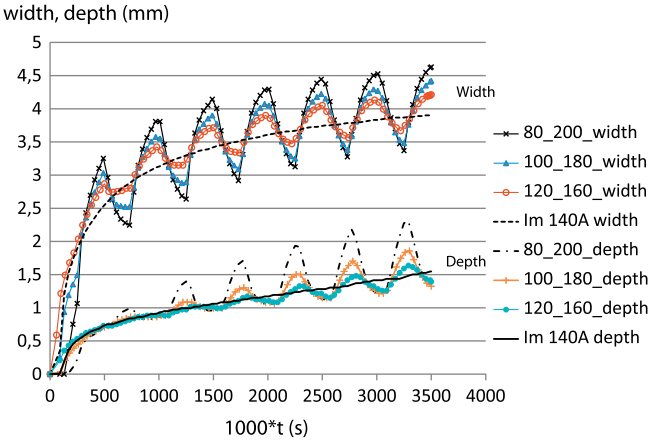

Fig. 15. Time evolution of weld pool dimensions for the three different current ratios and the mean current.

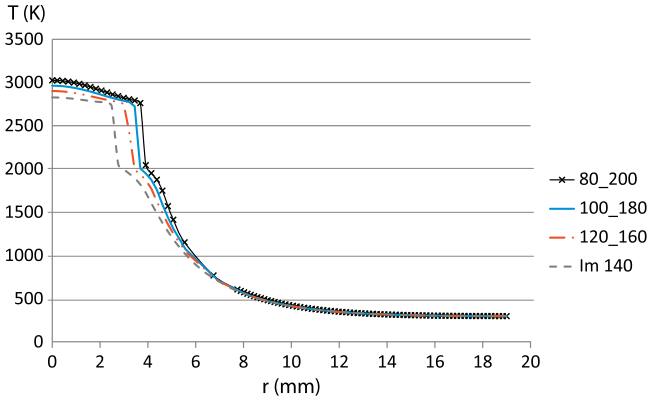

Fig. 16. Temperature at the top side of the plate for the three current ratios and the mean current at the end of calculation.

However thermal gradients tend to stabilize for the mean current after the time $t = 1$ s, while it continues to increase periodically for the three pulsed current cases. Thus, an optimal choice must be made between the weld pool penetration and the induced thermal gradients.

Fig. 18 shows the comparison between the experimental macrographs of the three pulsed current cases and the corresponding predicted weld pool shape after solidification. It shows a very good agreement as much as shape as dimensions. We could also see on the experimental macrographies the two solidification fronts corresponding to the final background and peak times.

3.3.2. *Influence of the pulse frequency at constant energy*

The variation of pulse frequency leads to control the heating period between bottom and peak welding currents. Then frequency controls thermal gradients and thus influences fluid flow in the weld pool. Using the 80/200 A rectangular current distribution previously used, with three different frequencies of 2, 4 and 6 Hz, we study the effect of the current frequency on the weld pool shape variation.

First, we start by comparing weld pool depth and width for each frequency. As seen in Fig. 19 the weld pool characteristics evolve at the same frequency as the corresponding welding current. As the previous studied cases, during the peak duration the weld pool width increases while the depth decreases and during the background duration the width decreases while the depth increases.

As regarding dimensions, the 2 Hz case produces a wider and deeper weld pool than the other frequencies, this seems to be

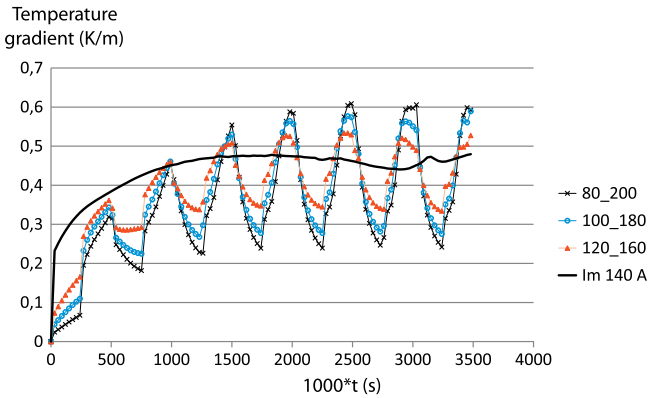

Fig. 17. Temperature gradients in the HAZ for the three current ratios and the mean current.

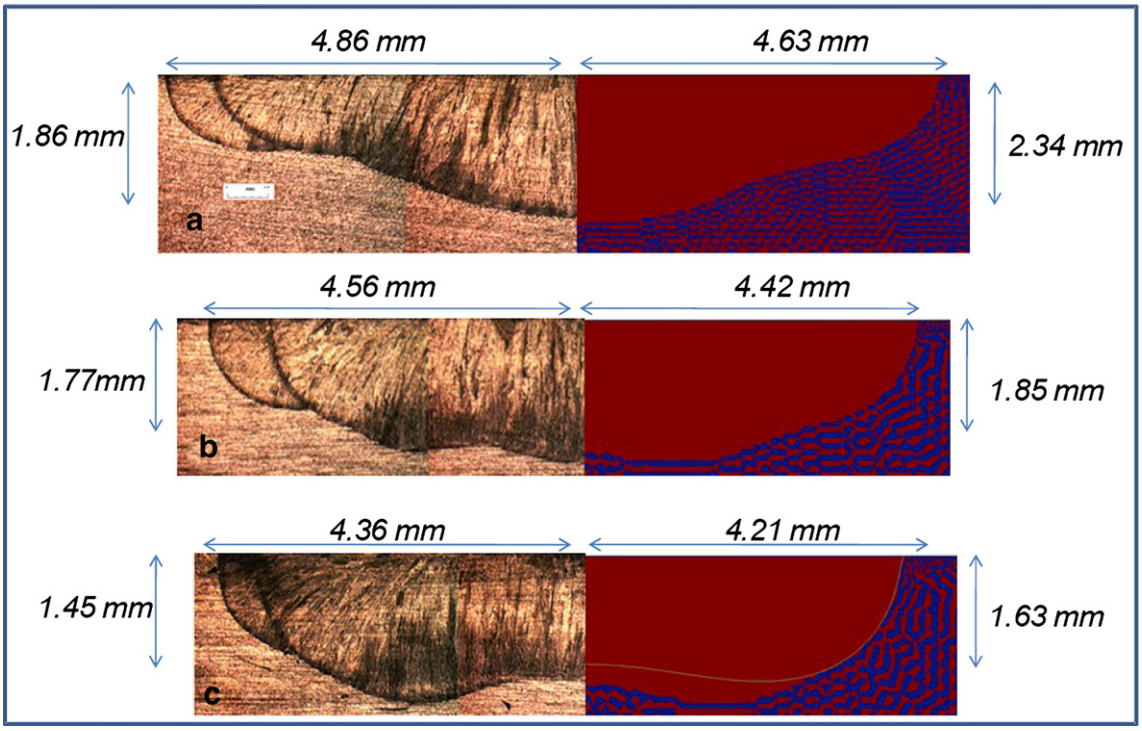

Fig. 18. Experimental macrographies and predicted weld pool shape; (a) 80/200 A, (b) 100/180 A, (c) 120/160 A.

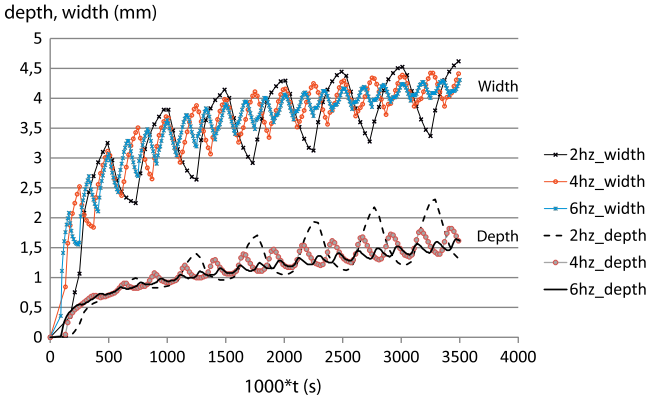

Fig. 19. Time evolution of weld pool dimensions for a 80/200 A pulsed current with three different pulse frequencies.

caused by the fact that the peak current is held during more time which causes an increasing of the weld pool temperature and thus dimensions. It is also important to notice that when we increase the frequency, the weld pool dimensions are more and more close to the mean current 140 A. The final computed weld pool shapes for each frequency are compared in Fig. 20, it goes with the previous remarks. This comparison is very interesting because we could get different weld pool shapes with the same welding energy simply by changing the pulse frequency.

The temperature evolution at the top side of the plate at the last increment of time is showed in Fig. 21. By comparing this figure to Fig. 16 we can see that the change in frequency has almost no effect on the final temperature at the top of the plate, that is not the case for the change in current ratio.

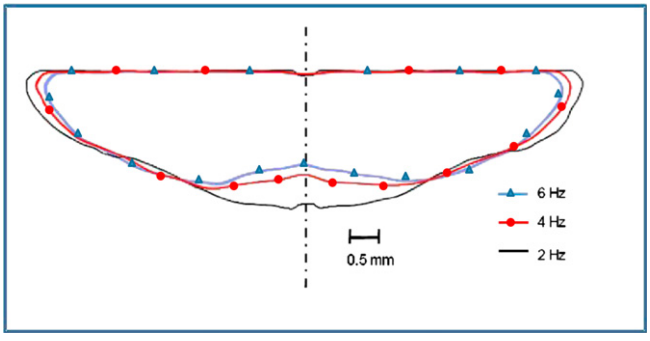

Fig. 20. Predicted weld pool shapes for a 80/200 A pulsed current welding with three different pulse frequencies.

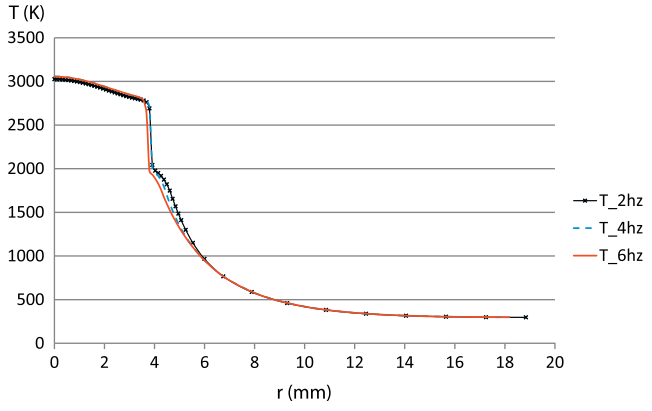

Fig. 21. Temperature at the surface for the three different pulse frequencies at the final time.

4. Conclusion

In this paper we have presented a heat transfer and fluid flow model for pulsed spot GTA welding. It deals with partially and fully penetrated weld pools. This model can explain the phenomena governing weld pool shape evolution. Moreover, it allows to study the influence of pulsed welding parameters on the final weld pool shape.

Gravity, electromagnetic forces, arc pressure and Marangoni effect are taken into account. Electromagnetism is solved using a magnetic field formulation which is easy to integrate in a finite element software. Surface tension gradient is temperature dependent and can be negative or positive according to the local temperature of AISI 304 stainless steel.

A numerical comparison between continuous current and pulsed current welding shows that pulsed welding can produce the same weld pool shape as continuous current with less welding energy. This shows the interest of pulsed current to limit the heat transferred to plate and then to reduce residual stress and distortions. The deformation of the free surface was also studied by stationary formulation, but it will be very interesting to develop a new dynamical free surface model that deals with the oscillations of the weld pool under the action of time-dependent arc pressure.

Finally, we use our model to estimate the influence of welding parameters such as current ratio and pulse frequency on the weld pool shape. It shows that for a stainless steel the choice of the peak current, background current and pulse frequency affects considerably the weld pool shape. Using a higher difference between the peak and background current results in a wider and deeper weld pool, but it also induces higher thermal gradient near the Heat Affected Zone. The model predictions are compared to different welding macrographs, it shows a very good prediction. Indeed with a unique surface tension gradient versus temperature relationship we have successfully predicted different weld pool geometries. It must be noticed that the sulfur activity, which governs the Marangoni effect, is a significant parameter for the final weld shape. This great influence of sulfur content is usually observed by welders.

References

[1] H.G. Fan, H.L. Tsai, S.Z. Na, Heat transfer and fluid flow in a partially or fully penetrated weld pool in gas tungsten arc welding. Int. J. Heat Mass Tran. 44 (2001) 417–428.
[2] S. Wang, J. Goldak, J. Zhou, S. Tchernov, D. Downey, Simulation on the thermal cycle of a welding process by space-time convection-diffusion finite element analysis. Int. J. Therm. Sci. 48 (2009) 936–947.
[3] J. Hu, H.L. Tsai, Heat and mass transfer in gas metal arc welding: part II. Int. J. Heat Mass Tran. 50 (2007) 833–846.
[4] F. Roger, K. Dang Van, Prediction of the weld shape in arc welding, a numerical modeling example in multiphysics coupling. Revue Européenne des elements finis 13 (2004) pp. 5–6–7.
[5] R.E. Leitner, G.H. McElhinney, E.L. Pruitt, An investigation of pulsed GTA welding variables. Weld. J., Res. Suppl. (1973) 405s–410s.
[6] H.R. Saedi, W. Unkel, Arc weld pool behavior for pulsed current GTAW. Weld. J., Res. Suppl. (1988) 247s–255s.
[7] P.R. Vishnu, W.B. Li, K.E. Easterling, Heat fluid model for pulsed welding. Mater. Sci. Technol. 7 (1991) 649–659.
[8] J. Scemeliovas, Determination of pulse current optimal parameters for manual arc welding. Mechanika 51 (2005) 66–69.
[9] W.H. Kim, S.J. Na, Heat and fluid flow in pulsed current GTA weld pool. Int. J. Heat Mass Tran. 41 (1998) 3213–3227.
[10] C.S. Wu, W. Zheng, L. Wu, Modelling the transient behaviour of pulsed current tungsten-inert-gas weldpools. Modelling Simul. Mater. Sci. Eng. 7 (1999) 15–23.
[11] P. Sahoo, T. DebRoy, M.T. McNallan, Surface tension of binary metal surface active solute systems under conditions relevant to welding metallurgy. Metall. Trans. B 19B (1988) 483–491.
[12] T. Zacharia, S.A. David, J.M. Vitek, T. Debroy, Weld pool development during GTA and laser beam welding of type 304 stainless steel, part I: theoretical analysis. Weld. J, Res. Suppl. (1989) 499s–509s.
[13] M.T. Mcnallan, H.G. Fan, T. DebRoy, Metall. Trans. B 22B (1991) 557.

Nomenclature

A_γ *[N m^{-1} K^{-1}]:* constant in surface tension gradient
B_θ *[Wb m^{-2}]:* azimuthal magnetic field
C_p *[Wb m^{-2}]:* specific heat
C_p^{eq}*[J kg^{-1} K^{-1}]:* equivalent specific heat
F_v*[N m^{-3}]:* body forces in the weld pool
I [A]: welding current
I_b *[A]:* background current
I_m *[A]:* mean current
I_p *[A]:* peak pulse current
L_{ref} *[m]:* reference length
P_a *[Pa]:* arc pressure
R_g *[J kg^{-1} mole^{-1} K^{-1}]:* gas constant
V_{ref} *[m s^{-1}]:* reference velocity
ΔH_0 *[J kg^{-1} mole^{-1}]:* standard heat of adsorption
Γ_s *[J kg^{-1} mole^{-1} m^{-2}]:* specific heat
β *[K^{-1}]:* coefficient of thermal expansion
$\frac{\partial\gamma}{\partial T}$*[N m^{-1} K^{-1}]:* surface tension gradient
ϵ_0 *[J kg^{-1} K^{-1}]:* vacuum permittivity
γ *[N m^{-1}]:* surface tension
γ_m *[N m^{-1}]:* surface tension at melting point
λ *[Pa]:* Lagrange multiplier
μ *[kg m^{-1} s^{-1}]:* dynamic viscosity
μ_0 *[H m^{-1}]:* magnetic constant
ϕ*[m]:* vertical displacement of the top surface
ρ *[kg m^{-3}]:* density
σ *[S m^{-1}]:* electrical conductivity
θ*:* dimensionless temperature
α_s *[weight%]:* activity of sulfur
f [Hz]: pulse frequency
f_L*:* liquid fraction
g [N kg^{-1}]: gravity constant
h_0 *[W m^{-2} K^{-2}]:* heat transfer coefficient
j_0 *[A m^{-2}]:* current density distribution at the top surface
j_r *[A m^{-2}]:* radial current density
j_z *[A m^{-2}]:* axial current density
k [W m^{-1} K^{-1}]: thermal conductivity
k_1*:* constant related to entropy of segregation
t_b *[s]:* background time
t_p *[s]:* peak pulse time
t_t *[s]:* total heating duration
u [m s^{-1}]: radial velocity
v *[m s^{-1}]:* axial velocity